# No evidence for passivation effects of Na and K at grain boundaries in polycrystalline $Cu(In,Ga)Se_2$ thin films for solar cells

Daniel Abou-Ras[1], Aleksandra Nikolaeva[1], Sebastián Caicedo Dávila[1], Maximilian Krause[1], Harvey Guthrey[2], Mowafak Al-Jassim[2], Marcin Morawski[3], Roland Scheer[3]

[1] Helmholtz-Zentrum Berlin für Materialien und Energie GmbH, Hahn-Meitner-Platz 1, 14109 Berlin, Germany
[2] National Renewable Energy Laboratory, 15013 Denver West Pkwy, Golden, CO 80401, USA
[3] Institute of Physics, Martin-Luther-University Halle-Wittenberg, 06120 Halle, Germany

Corresponding author: daniel.abou-ras@helmholtz-berlin.de

Abstract:
Thin-film solar cells based on $Cu(In,Ga)Se_2$ absorber layers have reached conversion efficiencies of well above 20%. One key of this success is the incorporation of alkali metals such as Na and K into the surface and the volume of the $Cu(In,Ga)Se_2$ thin film. The present work discusses the impact of Na and K on the grain-boundary (GB) properties in $Cu(In,Ga)Se_2$ thin films, i.e., on the barriers for charge carriers, $\Phi_b$, and on the recombination velocities at the GBs, $s_{GB}$. The authors first revise the physics connected with these two quantities as well as their impact on the device performance, and then provide values for the barrier heights and recombination velocities from the literature. The authors measured $s_{GB}$ values by means of cathodoluminescence analysis of Na-/K-free CIGSe layers as well as on CIGSe layers on Mo/sapphire substrates which were submitted to only NaF or only KF PDTs. Overall, passivating effects on GBs by neither Na nor K can be confirmed. The GB recombination velocities seem to remain on the same order of magnitude, in average about $10^3$-$10^4$ cm/s, irrespective of whether $Cu(In,Ga)Se_2$ thin films are Na-/K-free or Na-/K-containing.

## 1. Introduction

Currently, the solar-cell devices exhibiting highest conversion efficiencies of more than 23% have been fabricated using $Cu(In,Ga)Se_2$ (CIGSe) absorber layers which contain alkali metals already during growth or into which alkali metals were introduced via a postdeposition treatment (PDT) [1,2]. The impacts of the alkali metals Na, K, Rb, and Cs on the materials and device properties of CIGSe solar cells are diverse, and they can be divided into those present at the interfaces to the *n*-type buffer layer and to the back contact, as well as to those present at line and planar defects, of those particularly the ones at (random) grain boundaries (GBs). Moreover, it is appropriate to consider the effects of Na on the one hand and K on the other hand separately; while Na can occupy Cu sites in the CIGSe lattice easily, K cannot that easily owing to its large ion radii, which is why they rather segregate to extended structural defects or form precipitates [3].

It is well accepted that the main impact of Na on the CIGSe materials properties is the increase of the net doping from about $10^{14}$ $cm^{-3}$ to about $10^{15}$-$10^{16}$ $cm^{-3}$ [4]. Further influences of Na, especially on the growth process of the CIGSe absorber, were addressed in various publications (e.g., [5,6,7,8]) and will thus not be treated further in the present work. Recently, several reports highlighted the formation of noncontiguous (island-like) K-In-Se layers [9,10,11] at the CIGSe/buffer interface with thicknesses of few nanometers after KF

treatments. Therefore, it is assumed that the very thin, island-like K-In-Se layers passivate the corresponding interfaces, leading to reduced recombination, thus, to increased open-circuit voltage, without deteriorating the short-circuit current substantially.

In addition to these impacts, Na and K are also assumed to enhance the solar-cell performance via passivation of GBs (see, e.g., Ref. 3 and references therein). This assumption is based mainly on the fact that alkali metals were found to segregate at GBs [12,13] and that the presence of alkali metals in the CIGSe layer during its growth or via a post-deposition treatment leads to an increased open-circuit voltage ($V_{oc}$) [1], presumably owing to reduced nonradiative recombination at the GBs (while the $V_{oc}$ values are increased already by the presence of Na in the CIGSe layer due to the increase in the net-doping density, see above). It is noteworthy that in contrast to the CIGSe/buffer (or to the CIGSe/back contact) interfaces, alkali metals are not expected to form any secondary phases at GBs but rather contribute to the atomic / ionic reconstruction of the adjacent atomic planes at the GBs [14,15]. APT analyses determined the concentrations of Na and K at CIGSe GBs to about 0.1-1 at.% (order of magnitude) [16].

It should be noted that most analyses were conducted on CIGSe thin films on Mo/soda-lime glass (SLG) substrates. Since SLG contains Na as well as K oxides, both, Na and K, diffuse through the Mo layer into the growing CIGSe thin film, segregating to GBs (see, e.g., [12]). Therefore, in most studies, it is not possible to separate the Na and K effects at GBs.
In the present work, it will be shown that in spite of their contribution to the atomic / reconstruction at CIGSe GBs, there is no indication for a passivating effect of Na or K at these planar defects. Furthermore, it will be outlined to what extent Na as alkali metal may even contribute to the detrimental impact of GBs in CIGSe solar cells.

## 2. General situation at GBs in CIGSe thin films

As explained in detail already in a recent review on GBs in CIGSe layers [14], the two adjacent atomic planes of the neighboring grains at (random) GBs feature (owing to the atomic/ionic reconstruction) a high density of point defects in the highly compensated semiconductor CIGSe, involving matrix as well as impurity atoms, i.e., they are confined within very narrow GB regions with widths of smaller than 1 nm [17,18]. Owing to these small widths of the GB regions, within which the composition changes always differently for different GBs, band offsets in the valence or conduction bands and corresponding consequences for the electrical properties of GBs can be neglected.

Nevertheless, the segregated point defects localized at GBs may impact the electrical / optoelectronic properties of CIGSe thin films and thus of the corresponding solar cells in two different ways.

a) Effects on barriers for charge carriers
We may assign to a localized density of point defects at a given GB a corresponding density of defect states $N_{it}$ (given in $cm^{-2}$). Let $N_{it}$* be the net charge density of these defects with $N_{it}$* $\leq N_{it}$; note that defects are charged or neutral depending on the whether or not the Fermi level is larger than their energy. The free charge carriers in the *p*-type CIGSe layer screen this charge density, forming either a depletion region around the GB for a positive excess charge density or leading to accumulation of the free holes for a negative excess charge density. Consequently, according to Poisson's equation, the valence and conduction bands are bent

downwards or upwards. As described in detail by Seto [19], the heights of these barriers for holes or electrons can be calculated via

$$\Phi_b = ed^2 N_A / 8\varepsilon_r\varepsilon_0 \qquad (1)$$

for $N_A d < N_{it}$, where $N_A$ is the net doping density of the *p*-type CIGSe thin film, $d$ the average grain size in the polycrystalline layer, while $\varepsilon_r$ and $\varepsilon_0$ are the dielectric constants of the CIGSe layer and of the vacuum. In the regime of $N_A d < N_{it}$, the barrier height depends linearly on $N_A$. For $N_A d > N_{it}$, the dependency changes to

$$\Phi_b = eN_{it}^{*2} / 8\varepsilon_r\varepsilon_0 N_A \,. \qquad (2)$$

Setting $\varepsilon_r = 11.6$ [20] and $d$=0.5 µm for high-efficiency solar cells [21], the corresponding values for the barrier heights $\Phi_b$ are plotted in Figure 1, varying $N_{it}^*$ between 0.8 and $5\times10^{11}$ cm$^{-2}$ and $N_A$ between $1\times10^{13}$ and $1\times10^{18}$ cm$^{-3}$. It can be seen that for increasing net doping densities, $\Phi_b$ increases linearly until $N_A$ reaches about $10^{15}$-$10^{16}$ cm$^{-3}$, from where it decreases to much lower values.

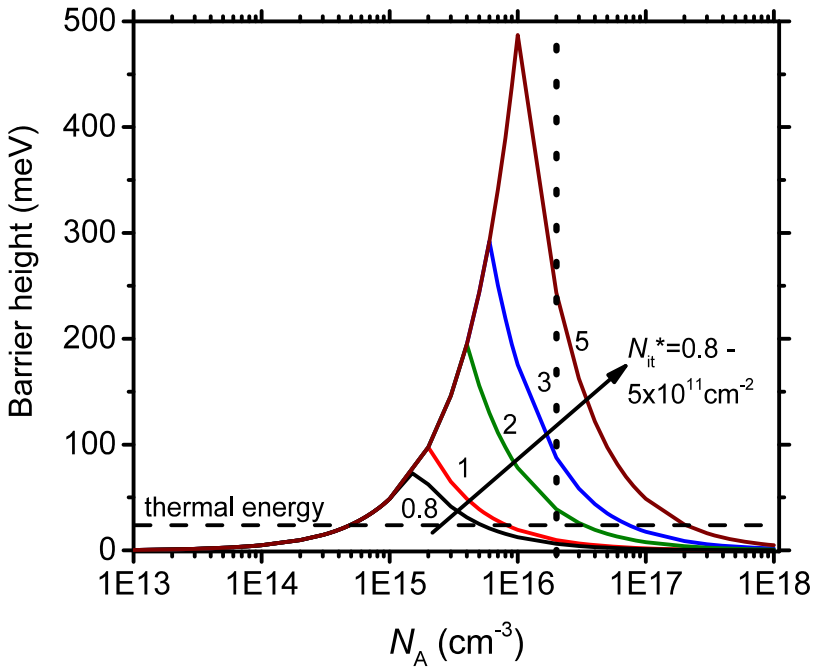


Figure 1: Barrier heights $\Phi_b$ as a function of the net-doping density $N_A$ (logarithmic scale), for various values of $N_{it}^*$ between 0.8 and $5\times10^{11}$ cm$^{-2}$, using Eqs. 1 and 2. The dashed horizontal line indicates the thermal energy $k_BT \approx 25$ meV ($k_B$ the Boltzmann constant, $T$ the absolute temperature), while the vertical dashed line marks the reported net-doping density of CIGSe in high-efficiency solar cells, $2\times10^{16}$ cm$^{-3}$.

When trying to estimate a reasonable range of the barrier heights $\Phi_b$ for high-efficiency CIGSe solar cells, we can look at their values for the reported net-doping density of such devices, about $2\times10^{16}$ cm$^{-3}$. From Figure 1, it is apparent that only for $N_{it}^*$ larger than about $2\times10^{11}$ cm$^{-2}$, substantial barriers form, which are larger than the thermal energy ($k_BT$). Moreover, it has to be taken into account that the upwards band bending at CIGSe GBs is limited by the Fermi level, which is positioned at about 100 meV above the valence-band edge for $N_A$=$2\times10^{16}$ cm$^{-3}$. In contrast, the downward band bending and therefore the

magnitude of the corresponding barrier height is per se not limited. Nevertheless, two-dimensional device simulations [22,23] suggest that (in order to obtain high-efficiency CIGSe devices), GBs barriers of larger than about -100 meV make no sense, since they lead (theoretically) to too strongly deteriorated device performances. Therefore, we assume that in high-efficiency CIGSe solar cells, the barrier heights at different GBs exhibit values varying between -0.1 and +0.1 eV, with average values of around 50 meV, and the corresponding $N_{it}^*$ values of about 2 to $3\times10^{11}$ $cm^{-2}$.

b) Effects on nonradiative recombination via trap states

Apart from barriers for charge carriers, the localized point defects at GBs lead also to charge-carrier-trapping defect states in the band gap, with trap-state densities of $N_{it}$. For the case of low injection, the effective recombination velocity at a given GB, $s_{GB}$, can be expressed as [24,25]

$$s_{GB} = 1/4\ N_{it}\ \sigma_{cap,e}\ v_{th} \exp(e\Phi_b/k_B T), \quad (3)$$

where $\sigma_{cap,e}$ is the capture cross-section for electrons (in $cm^2$), $v_{th}$ the thermal velocity for electrons, $1\times10^7$ cm/s, $k_B$ the Boltzmann constant, and $T$ the absolute temperature. Varying again $N_{it}$ between 0.8 and $5\times10^{11}$ $cm^{-2}$, as well as for $\Phi_b$=50-100 meV and $\sigma_{cap,e}$ $=1\times10^{-15}$ $cm^2$, $s_{GB}$ would take values ranging from $1\times10^3$ to $7\times10^4$ cm/s. Again by means of two-dimensional device simulations [22,23], it can be seen that such values lead to deteriorated device performances of CIGSe solar cells.

For high-injection conditions, Eq. 3 changes because there is hardly any bending of the conduction and valence bands (free electrons and holes exhibit about the same density), and moreover, the recombination is controlled by the hole caption [25]:

$$s_{GB} = 1/4\ N_{it}\ \sigma_{cap,h}\ v_{th}, \quad (4)$$

where it is assumed that electrons and holes exhibit the same thermal velocity $v_{th}$. Because of the vanishing band bending, the recombination velocity at GBs is considerably smaller than under low-injection conditions [25].

## 3. Experimental details

a) Production of the solar cells

A Na/K-free CIGSe absorber was deposited at University of Halle on a soda-lime glass (SLG) with sputtered Mo layer and $SiO_xN_y$ barrier to prevent Na/K out-diffusion during the three-stage process described elsewhere in detail [26]. The thickness of the CIGSe absorber layer was 2 µm as estimated from both, the laser-light scattering signal and glow discharge optical emission spectroscopy (GDOES). The same GDOES measurement was used also to confirm the lack of Na and K in the CIGSe layer. The solar cell was completed by the deposition of ~50 nm of CdS and ~500 nm of i-ZnO/ZnO:Al on top of the CIGSe/Mo/$SiO_xN_y$/glass stack. Moreover, a Ni/Al/Ni grid was evaporated on the solar-cell stack, and the active area defined by mechanical scribing.

Solar cells consisting of ZnO:Al/i-ZnO/CdS/CIGSe/Mo/SLG and ZnO:Al/i-ZnO/CdS/CIGSe/Mo/SLG (with Al grids on top of each) were produced at AIST, Tsukuba. After the CIGSe deposition by a three-stage process, the CIGSe layers were submitted to NaF

or KF PDTs (additional CIGSe/Mo/substrate stacks were held at the PDT temperature without any alkali flux, as references). The approximate thicknesses of the layers due to the NaF and KF PDTs were 1 and 20 nm). The conversion efficiencies of the CIGSe solar cells were measured under AM1.5G standard illumination at a light intensity of 0.1 W/cm$^2$

b) Conduction of the cathodoluminescence measurements

Cross-sectional specimens of completed CIGSe solar cells were prepared by face-to-face gluing of two stripes and by careful mechanical and Ar-ion polishing of the cross-section surface. A very thin (nominally 5 nm) carbon layer was deposited on the cross-section surface in order to reduce oxidation of the surface and drift during the measurements.

Plan-view specimens consisting of CIGSe/Mo/SLG and CIGSe/Mo/sapphire stacks were prepared for CL analysis by Ar+ ion milling with 3-kV accelerating voltage at an angle of ~4° with respect to the sample surface in order to remove the ZnO:Al/i-ZnO/CdS layers on top.
The hyperspectral cathodoluminescence (CL) images in the present work were acquired at a Zeiss Merlin scanning electron microscope (SEM) using a DELMIC SPARC CL (Kymera 193i spectrograph and an iDus InGaAs detector array from Andor) at room temperature, 8 kV, and 200pA/1nA (cross-section specimen), and on a JEOL JSM-7600FESEM equipped with a liquid-helium cryostage and spectrum-per-pixel acquisition capability, at 6 K, 5 kV, and 1.5 nA (plan-view specimens).

4. Role of Na and K at GBs

a) Effects on barriers for charge carriers

Since the main role of Na in CIGSe thin films is the increase of the net doping density from about $10^{14}$ cm$^{-3}$ to about $10^{15}$-$10^{16}$ cm$^{-3}$ [4], Eq. 1 suggests that Na-free CIGSe layers should exhibit very weak band bending at GBs. Indeed, results from scanning probe microscopy [27,28] provide evidence for small barriers at GBs (5-10 meV, order of magnitude) for charge carriers in the case of Na-free CIGSe layers, whereas these barriers reach values of up to ± 0.1 eV (order of magnitude) for Na-containing CIGSe thin films, as expected from Eq. 2 (see also the discussion in Sec. 2a). Therefore, while the presence of Na in CIGSe leads to a higher voltage of the corresponding solar cells via increased net doping density, at the same time, the $V_{oc}$ of the devices is limited by the substantial barriers at the GBs for the charge carriers.

It should be noted that although scanning Kelvin-probe force microscopy (KPFM) has been applied in numerous research efforts for the determination of barrier heights via the differences in contact potential between GBs and grain interiors (e.g., Ref. [29]), unfortunately, this technique probes GB properties only at the very surface (not more than 2 nm) of the analyzed thin film, and the results are strongly affected by free-carrier, electrostatic screening and by the tip size [30]. Corresponding values for GB barrier heights at the film surface are probably not the same as the ones for GBs in the bulk of the thin film.

This bulk sensitivity is provided rather by conductive atomic force microscopy (c-AFM) at varying applied bias voltages, provided the measured current runs through the CIGSe layer; e.g., when contacting the Mo back contact and then the film surface via the AFM tip in a CIGSe/Mo/substrate stack. Indeed, absolute values for GB barrier heights determined by c-AFM are typically much smaller (< 0.1 eV [31]) than those measured by means of KPFM (up

to 0.4-0.5 eV [32]). Therefore, in the present work, we will consider realistic (maximum) barrier heights to be between about -0.1 and +0.1 eV (average values about ±50-60 meV).

While the role of Na on the barrier heights at CIGSe GBs can be outlined clearly via its impact on the net-doping density in the CIGSe layer, it remains unclear whether K affects the net-doping density of CIGSe thin films and therefore the barrier heights at GBs considerably. There are reports in the literature showing increased as well as decreased net-doping densities of CIGSe thin films owing to KF PDT; see the review by Muzzillo et al. [3] and references therein.

b) Effects on nonradiative recombination via defect states

Recombination velocities $s_{GB}$ at CIGSe GBs were determined from analyses employing electron-beam-induced current (EBIC) and CL measurements. Both techniques provide independently values for $s_{GB}$ on the order of $10^3$ cm/s for most GBs in Na/K-containing CIGSe [33,34]; we note that few of the $s_{GB}$ values reported are also on the order of $10^4$ cm/s. In a correlative microscopy analysis employing EBIC and CL together with electron backscatter diffraction on the identical CIGSe area, it was verified that similar $s_{GB}$ values were obtained from both, EBIC and CL data, acquired at the identical GBs [35]. This is, it was shown that both techniques are basically able to provide decent estimates (not very precise values!) for the recombination velocities, giving their orders of magnitude. Unfortunately, there are no reports available in the literature on recombination velocities at GBs in Na-/K-free CIGSe layers. Therefore, as a first step, we performed CL measurements on a Na/K-free CIGSe layer (without any PDT), embedded within a completed solar cell, see Figure 2. We note that the conversion efficiency of the solar cell was 10.5%, mainly due to the low open-circuit voltage of 510 mV. We extracted CL profiles across various GBs and simulated them using the model proposed by Mendis et al. [36]. In this model, it is proposed that the of the CL intensity $I(x)$ decreasing along the coordinate $x$ from the grain interiors to the GB (where $x$=0) can be approximated using the equation [36]

$$\ln(1 - I(x)/I_{GI}) = \ln(S / S+1) - x / L, \quad (5)$$

where $I_{GI}$ is the maximum CL intensity within one of the grains adjacent to the GB, and $S = s_{GB} / L$ ($\tau$ and $L$ are the electron lifetime and diffusion length in the CIGSe layer). While $S$ (and thus $s_{GB}$) and $L$ are results of the linear fitting routine, the lifetime $\tau$ needs to be determined by additional measurements, e.g., by means of time-resolved photoluminescence (TRPL) measurements [37] or by evaluating absolute intensities of photoluminescence analyses [38]. We used TRPL measurements to determine the electron lifetime in the Na/K-free CIGSe layer to about 10 ns. Using Eq. 5 on the data shown in Fig. 2, we found that the GB recombination velocities $s_{GB}$ ranged from 2 to $6\times10^3$ cm/s.

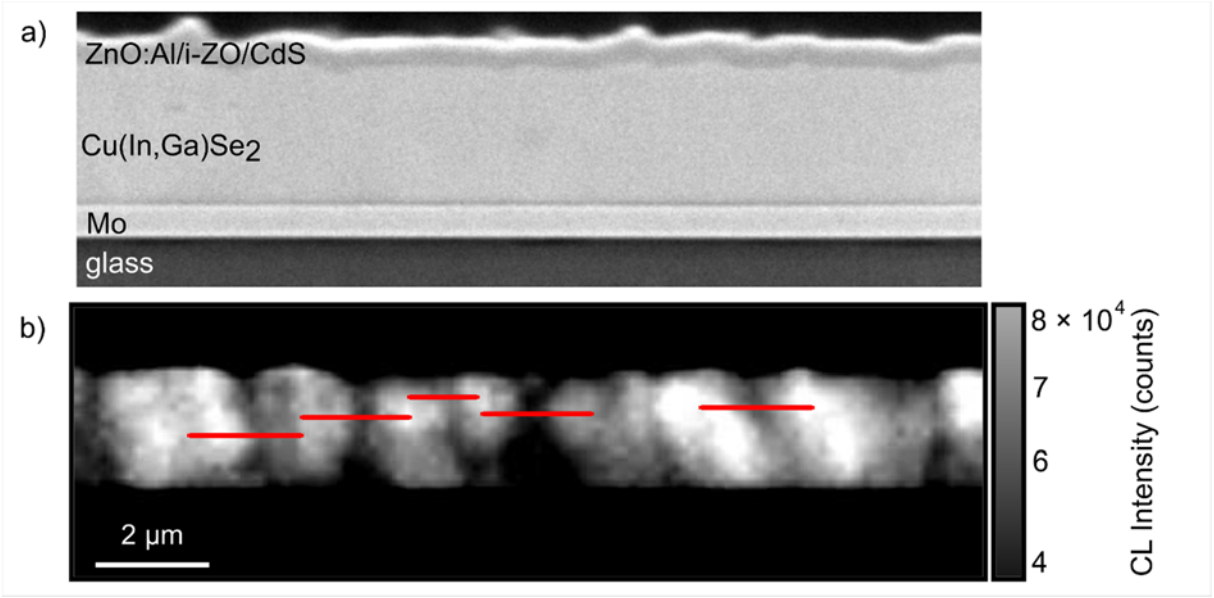


Figure 2: SEM image (a) and (b) panchromatic CL image, both acquired on the identical area of a cross-sectional ZnO:Al/i-ZnO/CdS/(Na free) CIGSe/Mo/glass specimen. CL profiles were extracted across various GBs (along the red lines). The calculated recombination velocities $s_{GB}$ ranged from 2 to $6\times10^3$ cm/s.

Since Na-free CIGSe layers exhibit a low net-doping density on the order of $10^{14}$ $cm^{-3}$, high-injection conditions for CL analyses are almost unavoidable. We repeated the CL measurements at 200 pA and determined similar recombination velocities at GBs as for the analysis at 1 nA. By estimating the density of electron-hole pairs generated by the electron beam via the equations provided by Maurice and Marfaing [39], it became clear that low-injection conditions for CL analyses of the Na-free CIGSe layer would only be achieved for beam currents of about 10 pA. However, beam currents of smaller than 100 pA resulted in CL images which exhibited a signal-to-noise level too low to evaluate $s_{GB}$ values accurately.

How can the GB signals acquired on the Na-free CIGSe layer under high-injection conditions and the resulting recombination velocities be related to corresponding signals and values under low-injection conditions? If we use Eq. 3 on GBs in the Na-free CIGSe layer, the exponential term containing the barrier height $\Phi_b$ becomes $\approx$1 since $\Phi_b$ is very small (5-10 meV) for a net-doping density of about $10^{14}$ $cm^{-3}$. Thus, the recombination velocities at GBs for Na-free CIGSe layers (with very low net-doping concentrations) are quite similar under low and high-injection conditions. This fact is corroborated also by the result that the CL intensities are still considerably lower at the GBs than in the grain interiors (Figure 2), even under apparent high-injection conditions.

Although we had performed CL measurements on a Na-/K-free CIGSe layer, the experimental evidence remains poor when considering the impact of the NaF and KF PDTs *separately* on the recombination velocities. This is, further measurements were necessary to obtain conclusive results on this matter. In a recent work, Guthrey et al. [40] studied GBs in CIGSe absorbers on sapphire (Na-free, K-free) and SLG substrates (Na-containing and K-containing) as well as with or without NaF or KF PDT by means of hyperspectral CL imaging. Qualitatively, their CL data indicate no substantial difference between Na/K-free and Na/K-containing CIGSe layers in terms of the detected CL contrast and thus of the enhanced nonradiative recombination at GBs. Since these authors did not extract any CL profiles across GBs nor calculated values for $s_{GB}$, we performed this evaluation in the present work. TRPL analyses (performed on CdS/CIGSe/Mo/substrate stacks) provided the electron

lifetimes in the CIGSe layers, and CL profiles across 20 GBs were evaluated using Eq. 5. We summarize all the investigated samples, the photovoltaic parameters, the net-doping densities in the CIGSe layers (taken from Ref. 40), as well as the electron lifetimes in Table 1. We note that we omitted on purpose the samples studied in Ref. 40 with combined NaF and KF PDTs, since we wanted to concentrate on individual effects of each alkali metal on the recombination velocities at GBs.

Table 1: Photovoltaic parameters ($V_{oc}$: open-circuit voltage, $j_{sc}$: short-circuit current density, *FF*: fill factor) of the solar cells as well as the net doping densities $N_A$ and the electron lifetimes $\tau$ in the studied CIGSe layers. Some values were taken from Ref. 40. We also give the average $s_{GB}$ values (horizontal lines in Fig. 4). It can be seen that $N_A$ is increased by one order of magnitude after the NaF PDT and KF PDT on sapphire substrates (Na-free and K-free). We note that the electron lifetimes in CIGSe layers on Mo/SLG and Mo/sapphire substrates differ by one order of magnitude.

| Sample | $V_{oc}$ (mV) | $j_{sc}$ (mA/cm$^2$) | *FF* | Efficiency (%) | $N_A$ (cm$^{-3}$) | $\tau$ (ns) | *Average* $s_{GB}$ (cm/s) |
|---|---|---|---|---|---|---|---|
| No PDT on sapphire | 522 | 30.3 | 0.59 | 9.4 | $2\times10^{14}$ | 2 | $8\times10^{3}$ |
| NaF PDT on sapphire | 619 | 30.1 | 0.70 | 13.0 | $3\times10^{15}$ | 2 | $1\times10^{4}$ |
| KF PDT on sapphire | 615 | 30.8 | 0.70 | 13.1 | $5\times10^{15}$ | 2 | $8\times10^{3}$ |
| No PDT on SLG | 718 | 31.9 | 0.79 | 18.1 | $5\times10^{15}$ | 21 | $2\times10^{3}$ |
| NaF PDT on SLG | 710 | 32.2 | 0.78 | 18.0 | $3\times10^{15}$ | 15 | $3\times10^{3}$ |
| KF PDT on SLG | 718 | 32.3 | 0.78 | 18.0 | $7\times10^{15}$ | 21 | $2\times10^{3}$ |

The CL maps of the samples listed in Table 1 are given in Figure 3, and the $s_{GB}$ values determined for 20 GBs in each of these samples are provided in the spreadsheet depicted in Figure 4. We can see that for the samples on sapphire, most of the $s_{GB}$ values remain in the range of $10^3$-$10^4$ cm/s, whereas for the CIGSe/Mo/SLG stacks, the recombination velocities at some of the CIGSe GBs are on the order of $10^2$ cm/s. Nevertheless, the *average* $s_{GB}$ values are on the order of $10^3$-$10^4$ cm/s, which is consistent with the results of precedent reports [33,34,35]. Moreover, there are no apparent positive influences of neither the NaF nor the KF PDT on recombination velocities at CIGSe GBs; it seems, actually, that the sGB values are even slightly larger for CIGSe with NaF PDT than for the "No PDT" or KF PDT samples. The $s_{GB}$ values always remain in similar ranges for samples on identical substrates, independently of whether no PDT, NaF PDT, or KF PDT was applied. We explain the differences between samples on sapphire and SLG by the different electron lifetimes (about one order of magnitude, see Table 1).

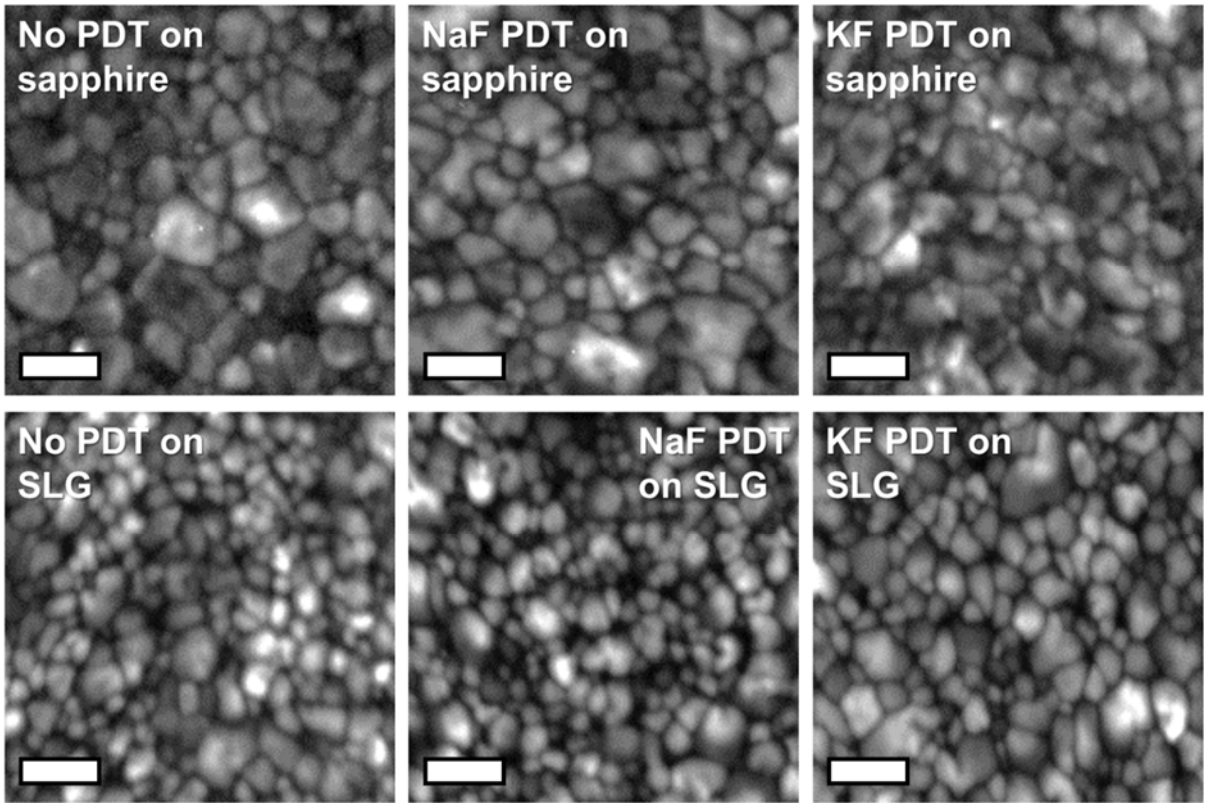


Figure 3: Plan-view CL intensity distribution maps (panchromatic) for the six samples listed in Table 1. The scale bars are 2 μm.

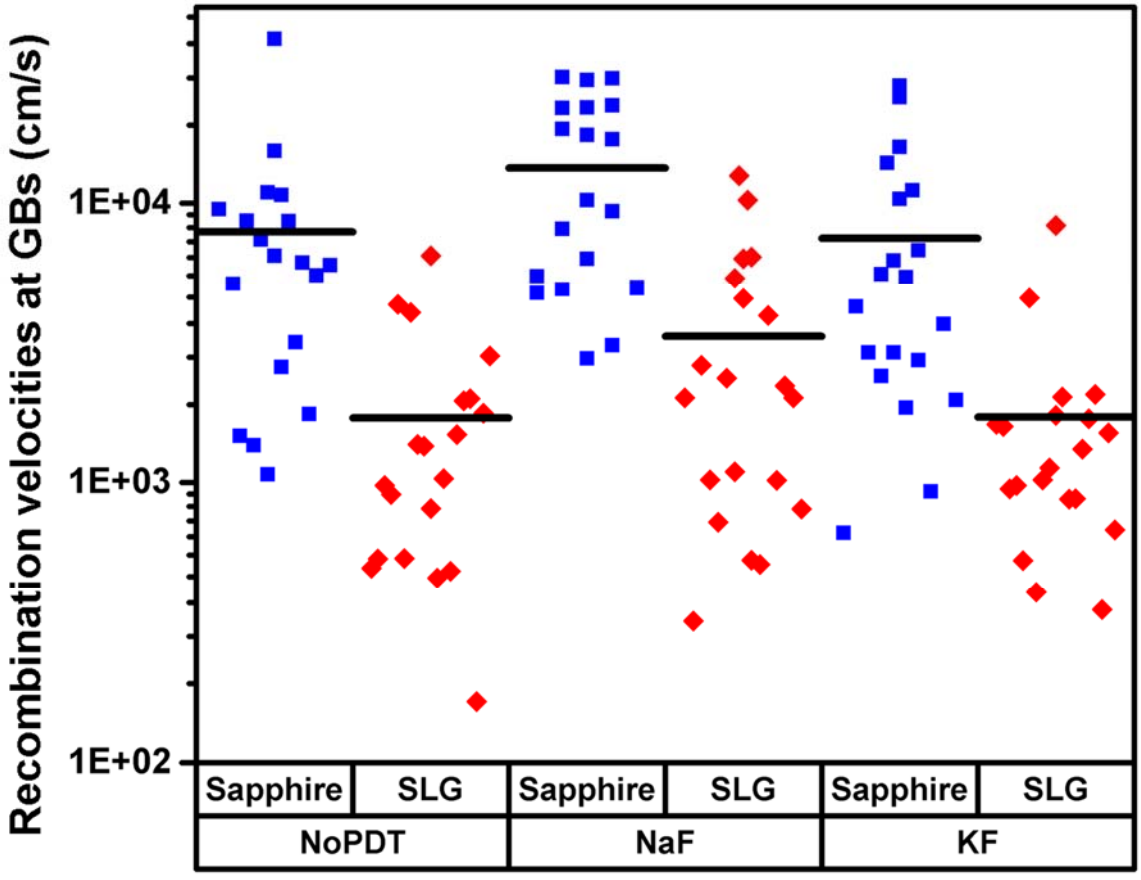

Figure 4: Recombination velocities obtained by extracting CL profiles across 20 GBs from the samples listed in Table 1 and by evaluating them using Eq. 5. The horizontal, black lines indicate the average $s_{GB}$ values for each sample.

## 5. Discussions

Taking all the available, experimental results together, we cannot identify any passivating effect of Na or K at CIGSe GBs. Considering the increased barrier heights at GBs for Na-containing CIGSe as compared with those of Na-free layers, Na exhibits - concerning the recombination activities at GBs - a rather detrimental influence. It is not clear in how far K or KF PDTs affect the barrier heights at GBs, since up to now, no conclusive effect of KF PDTs on the net-doping densities $N_A$ in CIGSe layers was demonstrated (see again Ref. 3 and the references therein), even if in the present work, the KF PDT exhibited a similar effect as the NaF PDT on the $N_A$ values in the CIGSe layers on Mo/SLG and Mo/sapphire substrates (see Table 1).

In spite of these considerable differences with respect to the barrier heights at GBs, similar recombination velocities at GBs were measured (when using the identical substrate, i.e., as in the present work, SLG or sapphire), irrespective of whether the polycrystalline CIGSe thin film was Na-/K-free or Na-/K-containing, with *average* $s_{GB}$ values on the order of $10^3$-$10^4$ cm/s. We note that the $s_{GB}$ values at individual GBs (Figure 4) overall exhibited magnitudes on a wide range with orders of $10^2$-$10^4$ cm/s. This finding can be linked to the mechanism of atomic/ionic reconstruction at CIGSe GBs described in Refs. 14 and 15. The result of this reconstruction is a residual density of point defects, which is always composed differently for different GBs (and thus, also the magnitude and sign of its excess charge density is different). Therefore, also the barrier heights and the recombination velocities at the GBs can be expected to be (largely) different. Still, similar *average* $s_{GB}$ values are found, which are not changed significantly by the absence/presence of neither Na nor K.

We can use Eqs. 1-3 to elucidate possible ways to reduce nonradiative recombination at CIGSe GBs. We will discuss each quantity contributing to these equations separately.

a) Decrease the localized defect density at GBs, $N_{it}$. Such a decreased density by the presence of alkali metals is not expected. Increased densities of impurities should rather increase the density of point defects segregating to the grain boundaries. Moreover, alkali metals on a vacant Cu site (e.g. $Na_{Cu}$) do not lead to charge-neutral defect states; the electronegativities of alkali metals (0.93 and 0.82 for Na and K) are smaller than that of Cu (1.9), and therefore, the defects act as weak donors.

b) Very low (about $10^{14}$ $cm^{-3}$) or very large (about $10^{17}$-$10^{18}$ $cm^{-3}$) net-doping densities $N_A$. In general, higher net-doping densities in the CIGSe layers lead to increased open-circuit voltages $V_{oc}$ of the corresponding solar cells via increased quasi-Fermi-level splitting. However, the increase of the net-doping density via introduction of higher concentrations of Na during the growth of during the PDT is limited by the solubility of Na in CIGSe (about $10^{-4}$ to $10^{-3}$ [41]). Much less impact due to even smaller solubilities can be expected by K diffusion into the CIGSe lattice. Instead, in order to obtain CIGSe layers with very high net-doping densities of $10^{17}$-$10^{18}$ $cm^{-3}$, the integral [Cu]/([In]+[Ga]) ratio of the produced CIGSe thin film needs to be very close to 1.

c) Decrease of the capture cross-sections $\sigma_{cap,e}$ / $\sigma_{cap,h}$ for electrons or holes. Their terms in Eqs. 3 and 4 exhibit a linear dependency of the recombination velocity $s_{GB}$. If impurities diffused to the CIGSe GBs forming point defects which reduce the average capture cross-sections considerably, consequently, the average $s_{GB}$ value would be decreased.

## 6. Conclusions

In the present work, we discussed the impact of the alkali metals Na and K on GB properties in polycrystalline CIGSe layers for corresponding solar cells. Overall, we can not confirm any passivating effect of neither Na nor K at CIGSe GBs. This is in contrast to the (presumably) confirmed influence of K on the passivation of the interfaces to the back contact and to the *n*-type buffer layer. With respect to the recombination velocities $s_{GB}$ at CIGSe GBs, their average values remain on the same order of magnitude, about $10^3$-$10^4$ cm/s, irrespective of whether or not the CIGSe layer contains Na or K. We attribute this paramount behavior of CIGSe GBs to the atomic/ionic reconstruction occurring in the two atomic planes adjacent to the GB plane, which results in residual defect concentrations $N_{it}$ at GBs, leading to similar recombination velocities.

## Acknowledgements

The authors are grateful for financial support by the Helmholtz Virtual Institute "Microstructure Control for Thin-Film Solar Cells" (VH-VI-520), the Helmholtz International Research School HI-SCORE (HIRS-0008), the Graduate School HyPerCells, and the BMWi project EFFCIS (No. 03240768B and 03240768C). Also, the authors are indebted to The authors thank Dr. Jiro Nishinaga and Mr. Hideki Takahashi of the Research Center for Photovoltaics at the National Institute of Advanced Industrial Science and Technology (AIST), Tsukuba, Japan, for fabricating CIGSe solar cells for the present work. Special thanks are due to Ulli Bloeck, HZB, for the SEM specimen preparation.

## References

[1] P. Jackson, R. Wuerz, D. Hariskos, E. Lotter, W. Witte, M. Powalla, *Phys. Stat. Solidi (RRL)* **2016**, *10*, 583.
[2] Press release: http://www.solar-frontier.com/eng/news/2019/0117_press.html (accessed on March 15, 2019).
[3] C.P. Muzillo, *Sol. En. Mater. Sol. Cells* **2017**, *172*, 18.
[4] F. Pianezzi, P. Reinhard , A. Chirilă, B. Bissig , S. Nishiwaki , S. Buecheler, A.N. Tiwari, *Phys. Chem. Chem. Phys.* **2014**, *16*, 8843.
[5] L. Kronik. D. Cahen, H.W. Schock, *Adv. Mater.* **1998**, *10*, 31.
[6] M. Bodegård, K. Granath, L. Stolt, *Thin Solid Films* **2000**, *361-362*, 9.
[7] D. Rudmann, D. Brémaud, H. Zogg, A.N. Tiwari, *J. Appl. Phys.* **2005**, *97*, 084903.
[8] F. Hergert, S. Jost, R. Hock, M. Purwins, J. Palm, *Thin Solid Films* **2007**, *517*, 5843.
[9] E. Handick, P. Reinhard, R.G. Wilks, F. Pianezzi, T. Kunze, D. Kreikemeyer-Lorenzo, L. Weinhardt, M. Blum, W. Yang, M. Gorgoi, E. Ikenaga, D. Gerlach, S. Ueda, Y. Yamashita, T. Chikyow, C. Heske, S. Buecheler, A.N. Tiwari, M. Bär, *ACS Applied Materials & Interfaces* **2017**, *9*, 3581.

[10] O. Donzel-Gargand, T. Thersleff, J. Keller, T. Törndahl, F. Larsson, E. Wallin, L. Stolt, M. Edoff, P*rog. Photovolt.* **2018**, *26*, 730.
[11] N. Nicoara, Th. Lepetit, L. Arzel, S. Harel, N. Barreau, S. Sadewasser, *Sci. Rep.* **2018**, *7*, 41361.
[12] O. Cojocaru-Mirédin, T. Schwarz, D. Abou-Ras, *Scripta Mater.* **2017**, *148*, 106.
[13] M. Raghuwanshi, A. Vilalta-Clemente, C. Castro, S. Duguay, E. Cadel, P. Jackson, D. Hariskos, W. Witte, P. Pareige, *Nano Energy* **2019**, *60*, 103.
[14] D. Abou-Ras, S. Schmidt, R. Caballero, T. Unold, H.-W. Schock, C. Koch, B. Schaffer, M. Schaffer, P. Choi, O. Cojocaru-Mirédin, *Adv. En. Mater.* **2012,** *2*, 992.
[15] D. Abou-Ras, S.S. Schmidt, N. Schäfer, J. Kavalakkatt, T. Rissom, T. Unold, R. Mainz, A. Weber, T. Kirchartz, E. Simsek Sanli, P.A. van Aken, Q.M. Ramasse, H.-J. Kleebe, D. Azulay, I. Balberg, O. Millo, O. Cojocaru-Mirédin, D. Barragan-Yani, K. Albe, J. Haarstrich, C. Ronning, *Phys. Stat. Sol. (RRL)* **2016**, *10*, 363.
[16] C.P. Muzzillo, J.D. Poplawsky, H.M. Tong, W. Guo, T. Anderson, *Prog. Photovolt.* **2018**, *26*, 825.
[17] D. Abou-Ras, B. Schaffer, M. Schaffer, S. Schmidt, R. Caballero, T. Unold, *Phys. Rev. Lett.* **2012,** *108*, 075502.
[18] E. Simsek Sanli, Q.M. Ramasse, W. Sigle, D. Abou-Ras, R. Mainz, A. Weber, H.-J. Kleebe, P.A. van Aken, *J. Appl. Phys.* **2016**, *120*, 205301.
[19] J.Y.W. Seto, *J. Appl. Phys.* **1975**, *46*, 5247.
[20] P.W. Li, R.A. Anderson, R.H. Plovnick, *J. Phys. Chem. Solids* **1979**, *40*, 333.
[21] M. Krause, A. Nikolaeva, M. Maiberg, P. Jackson, D. Hariskos, W. Witte, J.A. Márquez Prieto, S. Levcenko, T. Unold, R. Scheer, D. Abou-Ras, submitted.
[22] M. Gloeckler, J.R. Sites, W.K. Metzger, *J. Appl. Phys.* **2005,** *98*, 113704.
[23] K. Taretto, U. Rau, *J. Appl. Phys.* **2008,** *103*, 094523.
[24] C.H. Seager, *J. Appl. Phys.* **1982**, *53*, 5968.
[25] R. Brendel, *Thin-film crystalline silicon solar cells: physics and technology*, John Wiley & Sons, **2003**.
[26] E. Jarzembowski, M. Maiberg, F. Obereigner, K. Kaufmann, S. Krause, R. Scheer, *Thin Solid Films* **2015**, *576*, 75.
[27] Y. Yan, C.-S. Jiang, R. Noufi, S.-H. Wei, H. R. Moutinho, M. M. Al-Jassim, *Phys. Rev. Lett.* **2007,** *99*, 235504.
[28] D. Azulay, D. Abou-Ras, I. Popov, I. Balberg, O. Millo, *phys. stat. sol. (RRL)* **2016**, *10*, 448.
[29] S. Sadewasser, T. Glatzel, S. Schuler, S. Nishiwaki, R. Kaigawa, M.Ch. Lux-Steiner, *Thin Solid Films* **2003**, *431-432*, 257.
[30] Y. Rosenwaks, R. Shikler, T. Glatzel, S. Sadewasser, Phys. Rev. B **2004**, 70, 085320.
[31] S.Sadewasser, D.Abou-Ras, D. Azulay, R. Baier, I. Balberg, D. Cahen, S. Cohen, K. Gartsman, K. Ganesan, J. Kavalakkatt, W. Li, O. Millo, T. Rissom, Y. Rosenwaks, H.-W. Schock, A. Schwarzman, T. Unold, *Thin Solid Films* **2011**, *519*, 7341.
[32] R. Baier, C. Leendertz, D. Abou-Ras, M.C. Lux-Steiner, S. Sadewasser, *Sol. En. Mater. Sol. Cells* **2014**, *130*, 124.
[33] M. Nichterwitz, D. Abou-Ras, K. Sakurai, J. Bundesmann, T. Unold, R. Scheer, H.-W. Schock, *Thin Solid Films* **2009**, *517*, 2554.
[34] A. Nikolaeva, M. Krause, N. Schäfer, W. Witte, D. Hariskos, T. Kodalle, C. Kaufmann, N. Barreau, J.A. Marquez Prieto, S. Levcenko, D. Abou-Ras, submitted.
[35] D. Abou-Ras, N. Schäfer, T. Rissom, M.N. Kelly, J. Haarstrich, C. Ronning, G.S. Rohrer, A.D. Rollett, *Acta Mater.* **2016**, *118*, 244.
[36] B.G. Mendis, L. Bowen, Q.Z. Jiang, *Appl. Phys. Lett.* **2010**, *97*, 092112.
[37] R.K. Ahrenkiel, *Solid-State Electronics* **1992**, *35*, 239.

[38] C. J. Hages, A. Redinger, S. Levcenko, H. Hempel, J.M. Koeper, R. Agrawal, D. Greiner, C.A. Kaufmann, T. Unold, *Adv. Energy Mater.* **2017**, *7*, 1700167.
[39] J.L. Maurice, Y. Marfaing, *J. Phys. IV* **1991**, *C6*, 77.
[40] H. Guthrey, J. Moseley, J. Nishinaga, H. Shibata, H. Takahashi, M. Al-Jassim, *IEEE J. Photovolt.* **2018**, *8*, 1833.
[41] R.V. Forest, B.E. McCandless, X. He, A.A. Rockett, E. Eser, K.D. Dobson, R.W. Birkmire, *J. Appl. Phys.* **2018**, *121*, 245102.